

# **Electron Microscopic Evaluation and Fission Product Identification of Irradiated TRISO Coated Particles from the AGR-1 Experiment: A Preliminary Study**

**HTR 2012**

I.J. van Rooyen  
D.E. Janney  
B.D. Miller  
P.A. Demkowicz  
J. Riesterer

**October 2012**

This is a preprint of a paper intended for publication in a journal or proceedings. Since changes may be made before publication, this preprint should not be cited or reproduced without permission of the author. This document was prepared as an account of work sponsored by an agency of the United States Government. Neither the United States Government nor any agency thereof, or any of their employees, makes any warranty, expressed or implied, or assumes any legal liability or responsibility for any third party's use, or the results of such use, of any information, apparatus, product or process disclosed in this report, or represents that its use by such third party would not infringe privately owned rights. The views expressed in this paper are not necessarily those of the United States Government or the sponsoring agency.

The INL is a  
U.S. Department of Energy  
National Laboratory  
operated by  
Battelle Energy Alliance



## Electron Microscopic Evaluation and Fission Product Identification of Irradiated TRISO Coated Particles from the AGR-1 Experiment: A Preliminary Review.

IJ van Rooyen, DE Janney<sup>1</sup>, BD Miller<sup>1</sup>, PA Demkowicz<sup>1</sup>, J. Riesterer<sup>1,2</sup>  
Idaho National Laboratory  
Idaho Falls, ID 83415-6188, USA  
phone: +1-208-533-7199, isabella.vanrooyen@inl.gov

<sup>1</sup>Idaho National Laboratory, Idaho Falls, ID 83415-6188, USA  
<sup>2</sup>FEI Company, 5350 Dawson Creek Dr., Hillsboro, OR 97124, USA

**Abstract** – Post-irradiation examination of coated particle fuel from the AGR-1 experiment is in progress at Idaho National Laboratory and Oak Ridge National Laboratory. In this paper a brief summary of results from characterization of microstructures in the coating layers of selected irradiated fuel particles with burnup of 11.3% and 19.3% FIMA will be given. The main objectives of the characterization were to study irradiation effects, fuel kernel porosity, layer debonding, layer degradation or corrosion, fission-product precipitation, grain sizes, and transport of fission products from the kernels across the TRISO layers. Characterization techniques such as scanning electron microscopy, transmission electron microscopy, energy dispersive spectroscopy, and wavelength dispersive spectroscopy were used. A new approach to microscopic quantification of fission-product precipitates is also briefly demonstrated. Microstructural characterization focused on fission-product precipitates in the SiC-IPyC interface, the SiC layer and the fuel-buffer interlayer. The results provide significant new insights into mechanisms of fission-product transport. Although Pd-rich precipitates were identified at the SiC-IPyC interlayer, no significant SiC-layer thinning was observed for the particles investigated. Characterization of these precipitates highlighted the difficulty of measuring low concentrations of Ag in precipitates with significantly higher concentrations of Pd and U. Different approaches to resolving this problem are discussed. An initial hypothesis is provided to explain fission-product precipitate compositions and locations. No SiC phase transformations were observed and no debonding of the SiC-IPyC interlayer as a result of irradiation was observed for the samples investigated. Lessons learned from the post-irradiation examination are described and future actions are recommended.

### I. INTRODUCTION

A series of irradiation experiments are planned in the Advanced Test Reactor (ATR) at Idaho National Laboratory (INL) to evaluate the performance of tristructural isotropic (TRISO) coated particle fuel as part of the Next Generation Nuclear Plant (NGNP) program [1]. AGR-1, the first

of these irradiation experiments, began in the ATR in December of 2006 and ended in November 2009. This paper represents the initial results obtained from the electron microscopic examination of selected irradiated TRISO coated particles (CPs) taken from AGR-1 fuel Compact 6-3-2 and Compact 4-1-1. The unique identification number (e.g. 6-3-2) is based on the specific capsule, level, and stack

number for each compact during the irradiation. Compact 6-3-2 refers to the compact in Capsule 6 at Level 3 of Stack 2. More details of the identification numbers, the AGR-1 irradiation capsules, and the NGNP PIE program are provided in Reference 2.

The main objective of the electron microscopic examination of fuel particles is to characterize microstructure to establish irradiation effects, fuel kernel porosity, layer degradation or corrosion, fission product precipitation, layer debonding, and grain size and boundary property determination. Migration of fission products from the kernels across the TRISO layers will also be evaluated. In particular, corrosion of the SiC layers by fission products such as palladium, resulting in localized layer thinning, will be investigated. Another objective is to determine if there are microstructure differences between particles that exhibited high and low releases of Ag-110m. In this paper, the interpretation and discussion of results obtained on the inner pyrolytic carbon (IPyC) and SiC layers will be the primary focus with more limited information on observed behavior of the fuel kernel.

## II. SAMPLE IDENTIFICATION AND METHODS USED

### II.A. Fuel particles and irradiation conditions

Compact 6-3-2 contains baseline fuel fabricated with coating process conditions similar to those used to fabricate historic German fuel because of its excellent irradiation performance with UO<sub>2</sub> kernels. The AGR-1 fuel is, however, made of low-enriched UCO (uranium oxycarbide). Kernel diameters are approximately 350 μm with a U-235 enrichment of approximately 19.7%. Along with the baseline fuel, the AGR-1 irradiation experiment also includes three different fuel variants [3]. Compact 4-1-1 contains variant 3 fuel. The variant 3 fuel carrier gas composition for the SiC layer deposition was changed from 100% hydrogen to a 50% argon-50% hydrogen mixture and the deposition temperature was lowered relative to the baseline (from 1500 to 1425°C). This change is expected to reduce the potential for SiC defects resulting from uranium dispersion and provide a variation in SiC microstructure that may be less permeable to metallic fission products. The irradiation parameters are shown in Table 1.

Table 1: Irradiation parameters for AGR-1 Compact 6-3-2 and Compact 4-1-1.

Parameter	Compact 6-3-2	Compact 4-1-1
% FIMA average burnup	11.3	19.3
Time-average, volume –average temperature (°C)	1070	1073
Time-average, maximum temperature (°C)	1144	1182
Average fast fluence E21 n/cm <sup>2</sup>	2.38	4.13
Fuel type	Baseline	Variant 3

### II.B. Selection of fuel particles

Because of the importance of silver behavior in TRISO fuel, specific particles were chosen for analysis as part of this study based on the degree of silver retention exhibited during irradiation. Individual particles from selected deconsolidated compacts were gamma counted to measure the activity of various gamma-emitting fission products [2]. Figures 1 and 2 show the fraction of retained Ag-110m in 60 particles from Compact 6-3-2 and 58 particles from Compact 4-1-1 respectively (detailed discussion of these figures and the method for calculating the fraction of retained Ag-110m is in Reference 2). Note that the particles with lower measured vs. calculated ratios (left side of the figures) apparently released a greater fraction of their silver inventory during irradiation compared to particles with higher ratios.

Four coated particles from Compact 6-3-2 were identified for electron microscopic examination based on results indicating that they had a retained Ag-110m inventory at the high end (CP34, CP35, CP39) and low end (CP30) of the population analyzed, as indicated in Figure 1. One particle from Compact 4-1-1 (CP21) with average Ag-110m retention was also analyzed as part of this study (Figure 2). The particles were mounted in a two-part epoxy and ground in most cases to a plane near the particle mid-plane, where final polish was then performed. Additional particles will be selected and analyzed in a similar manner in the future as part of this ongoing study of the irradiated AGR-1 fuel.

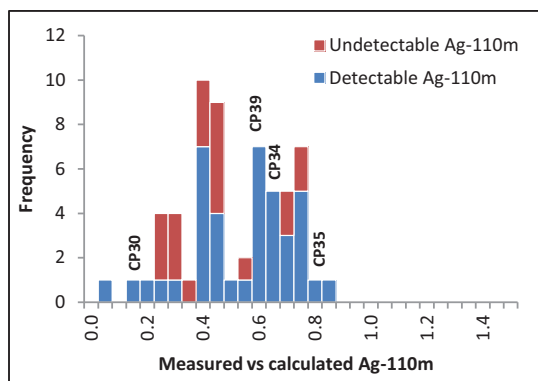


Figure 1: Ratio of measured to calculated Ag-110m activity for 60 particles from Compact 6-3-2. The locations of the four specific particles examined in this study are indicated on the distribution.

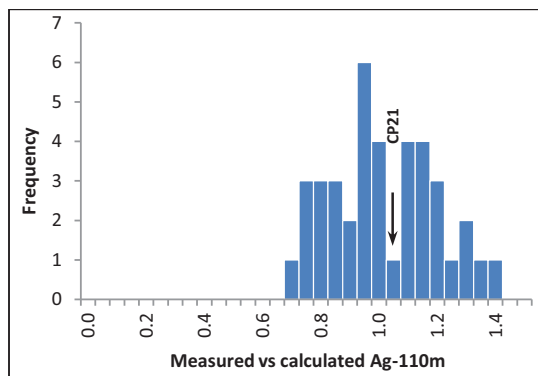


Figure 2: Ratio of measured to calculated Ag-110m activity for 58 particles from Compact 4-1-1. The location of CP21 examined in this study is indicated on the distribution.

### II.C. Approach to achieve microstructural objectives

A phased approach was used to achieve the microstructural characterization objectives. Initial screening and basic examination with a scanning electron microscope (SEM) identified specific areas or features of interest. A plan for SEM examination typically included identifying fission product precipitation, SiC attack, SiC grain sizes and grain boundary characteristics, and fuel kernel features. A transmission electron microscope (TEM) investigation plan was then prepared based on the knowledge gained from the basic SEM examination as shown in Figure 3. The TEM plan first identified the locations where samples for TEM examination would be prepared using the focused ion beam

(FIB), followed by more detailed studies during the TEM investigation. In Figure 3, specific TEM lamellas prepared with the FIB can be seen in several locations on the particle cross-section. Arrows indicate approximate locations where additional lamellae were prepared or planned. Note that the TEM examinations focus on the interface regions between coating layers, in particular the IPyC-SiC interface.

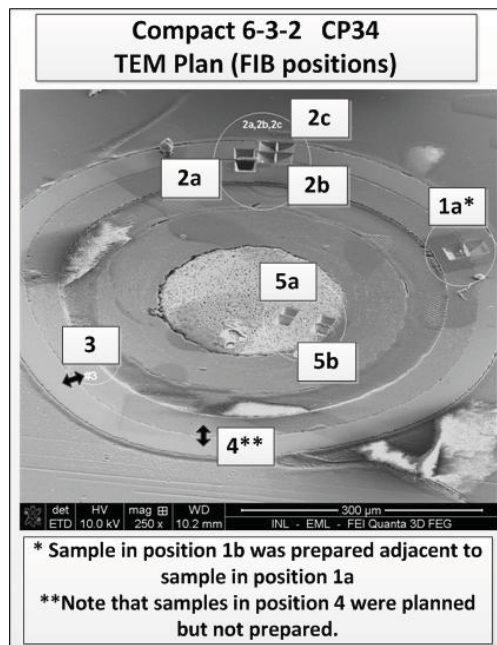


Figure 3: An example of a TEM examination plan for CP34 from Compact 6-3-2, based on SEM examination results.

Other advanced microscopic techniques, for example local electrode atom probe (LEAP), electron energy-loss spectroscopy (EELS), electron back scatter diffraction (EBSD) and high resolution transmission electron microscopy (HRTEM), are not included in this examination at present mainly because of challenges in sample preparation and transport of irradiated samples from one facility to another.

Numerous precipitates were observed in the coating layers during initial SEM characterization of the cross-sections. Precipitate characterization was done using scanning and transmission electron microscopy. SEM examination was used to identify the spatial distribution of the precipitates. SEM X-ray mapping was used to study the spatial distributions of elements and the morphology of the precipitates.

The FIB was used to prepare samples from selected areas for detailed examination in the TEM. Each TEM sample is approximately 10  $\mu\text{m}$  square and 100 nm thick, and has an original orientation perpendicular to the surface of the particle cross-section. Samples were prepared from the IPyC-SiC interface area, the inner part of the SiC layer, and the outer part of the SiC layer. TEM examination used a combination of electron diffraction, imaging, and energy-dispersive X-ray spectroscopy (EDX) to provide detailed information about the crystal structures of individual precipitates, their relationship to the surrounding matrix, and semi-quantitative chemical compositions.

### III. RESULTS AND DISCUSSION

#### III.A. Precipitate distribution

The precipitate location profile was investigated using an image montage. A montage was made by capturing sequential secondary electron images of the IPyC-SiC interface at 4000x magnification, and ensuring that there was adequate overlap between adjacent images to stitch them together. Adobe Photoshop was used to combine the images by overlapping shared features within images to form a complete image montage of the interface in order to visualize the location of precipitates around the entire particle circumference.

From each individual image, the interlayer thickness was measured from the SiC finger that extended the furthest into the IPyC to the portion of the SiC that receded the most, measured perpendicular to the interface as shown in Figure 4.

It is important to note that no standardized method to measure the IPyC-SiC interlayer thickness exists in the HTR research community. This approach was used for this evaluation as it provides a repeatable method for comparison purposes. This method may yield different interlayer thickness values depending on the magnification used to take the images (because of the different length of the interlayer used for measurement in each image). In this study a constant magnification was used for both particles characterized using this method in order to minimize the effect of image size.

The results from these measurements are provided in Table 2 for two of the particles analyzed in this study. The IPyC-SiC interlayer thickness for CP34 (Compact 6-3-2) varies from 0.7 to 3.7  $\mu\text{m}$ , with an average thickness of 1.7  $\mu\text{m}$ , while the thickness of CP21 (Compact 4-1-1) varies from 2.1 to 6.5  $\mu\text{m}$  with an average thickness of 3.7  $\mu\text{m}$ . It is not yet

clear whether this difference in thickness is significant for fission product transport or the formation of precipitates.

The distribution and position of the precipitates in the coating layers are also of interest as this may provide insight to the transport behavior of some fission products. Therefore, two measurements were performed and the results are presented here. Precipitates in the coating layers around the entire particle cross-section circumference were identified based on the light contrast areas on SEM images. SEM EDX analysis was used to identify similar features as Pd-rich precipitates in selected areas of the particle cross-sections.

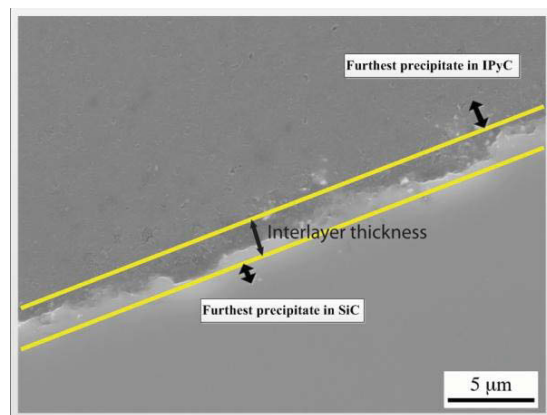


Figure 4: SEM image showing interlayer thickness measurement and schematic presentation to show measurement of furthest precipitate from interlayer.

Table 2: Interlayer thickness measurements of CP34 from Compact 6-3-2 and CP21 from Compact 4-1-1

IPyC-SiC Interlayer thickness ( $\mu\text{m}$ )	Compact 6-3-2 CP34	Compact 4-1-1 CP21
Average	1.7	3.7
Maximum	3.7	6.5
Minimum	0.7	2.1

The SEM results shown in Figures 5 and 6 indicate that the precipitates are distributed randomly around the full circumference of both coated particles investigated. The location of the precipitates does not appear to be significantly correlated with the kernel deformation and buffer fracture for CP21 from Compact 4-1-1 as shown in Figure 6. The furthest precipitate distance from the interface in both SiC and IPyC layers was measured for each image as schematically depicted in Figure 4. These results are presented in Table 3 and show that the precipitates in the SiC layer of CP34

(Compact 6-3-2) were at an average distance of 6.7  $\mu\text{m}$  from the IPyC-SiC interface but with a maximum distance of 15.3  $\mu\text{m}$ . The measurements in the IPyC revealed that the average distance is 2.9  $\mu\text{m}$  from the IPyC-SiC interface with a maximum distance of 15.3  $\mu\text{m}$ , suggesting that the interface and/or SiC-layer acts as an initial barrier to the transport/movement of these precipitates. No significant differences are noted comparing the distance of precipitates from the interface in the IPyC layer between the two compacts. The average and maximum penetration of precipitates in SiC are slightly larger for Compact 4-1-1. A larger coated particle sample set will be needed before more definitive conclusions can be drawn relative to potential operating conditions (time, burnup, temperature).

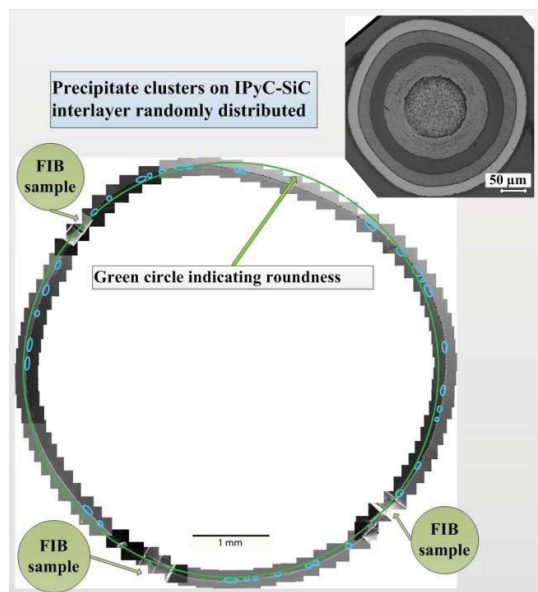


Figure 5: CP34 (Compact 6-3-2) SEM montage showing randomly distributed precipitate clusters encircled by blue. Inset image at upper right is an optical micrograph of the particle cross-section.

Table 3. Distance of precipitates from the IPy-SiC interlayer of CP34 from Compact 6-3-2 and CP21 from Compact 4-1-1.

	Compact 6-3-2 CP34	Compact 4-1-1 CP21
<b>Distance of precipitates in SiC (<math>\mu\text{m}</math>) from the interface</b>		
Average	6.7	9.3
Maximum	15.3	17.5
<b>Distance of precipitates in IPyC (<math>\mu\text{m}</math>) from the interface</b>		
Average	2.9	2.7
Maximum	15.3	16.4

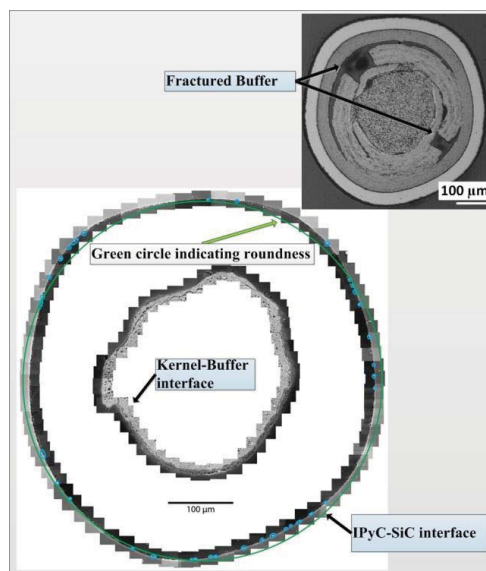


Figure 6: CP21 (Compact 4-1-1) SEM image and montage showing randomly distributed precipitate clusters encircled by blue. Inset image at upper right is an optical micrograph of the particle cross-section.

### III.B. Pd-rich Precipitate Identification

The approach followed for precipitate identification was to firstly identify the precipitate rich areas using SEM analysis. Secondly TEM samples were then prepared using FIB from areas where precipitate clusters were identified during the SEM evaluation. The initial SEM and TEM analyses of the specimens taken from these particles have focused on fission product precipitates in the various coating layers.

The precipitates shown in Figure 7 found in Positions 3 and 4 in CP34 were identified as Pd-rich during the initial SEM-EDX examination (Positions 3 and 4 correspond to the TEM positions identified in Figure 3). Interestingly, the Pd-rich precipitates in position 3 (Figure 7(a)) appear to be situated in SiC “fingers” while the Pd-rich precipitates in position 4 (Figure 7(b)) are in the IPyC layer as well. Characterization studies by Barrachin *et al.* [4] on HFR-EU1bis experiments (10.2% FIMA, calculated pebble center temperature of 1523 K) found that Pd is specifically present in the IPyC layer at the inside of the SiC layer, but no Pd is mentioned in the SiC layer itself. This study on CP34 shows in contrast that Pd precipitates are present in both the interlayer and in the SiC layer.

The TEM evaluation of CP34 is discussed here as an example. Figure 3 shows the positions where TEM samples were prepared using FIB. Qualitative

analyses of the TEM-EDX spectra showed significant concentrations of U, Pd, and Si, with some spectra obtained from the precipitates also having significant concentrations of Zr. C was also identified, but as IPyC and SiC contain high concentrations of C, it cannot be distinguished from any C in the precipitates themselves. The U-Pd-Si precipitates were observed at grain or phase boundaries near the IPyC-SiC interface in CP30, CP34, and CP35 of Compact 6-3-2 (Figures 8 to 11).

The majority of the precipitates that have been characterized are single crystals. Selected-area diffraction patterns were collected from numerous precipitates (e.g., Figure 12). All of the diffraction patterns could be indexed as  $UPd_2Si_2$  (tetragonal, space group  $I4/mmm$ ), and represented eight distinct zone axes. Some of the patterns had extra reflections that may either be from adjacent crystals or from double diffraction involving both a precipitate and the adjacent matrix. Proportions of U and Pd from EDX data are not consistent with  $UPd_2Si_2$ . Thus, it seems likely that the precipitates all represent a single phase, which is similar to  $UPd_2Si_2$  but does not have the stoichiometric composition.

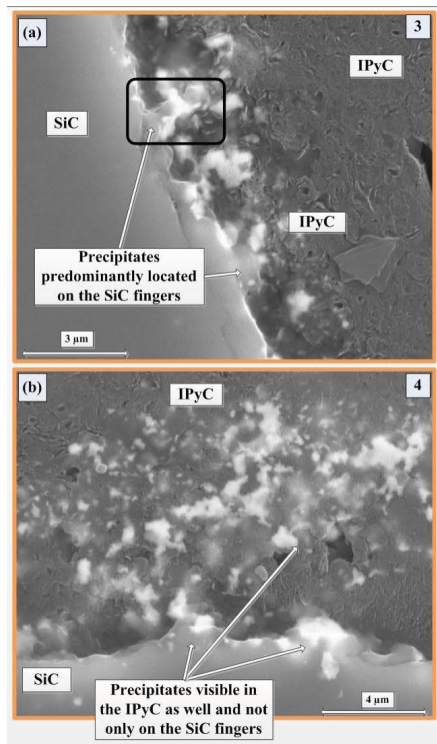


Figure 7: Pd-rich precipitates from two different positions on a cross section of CP34 (Positions 3 and 4 as shown in Figure 3).

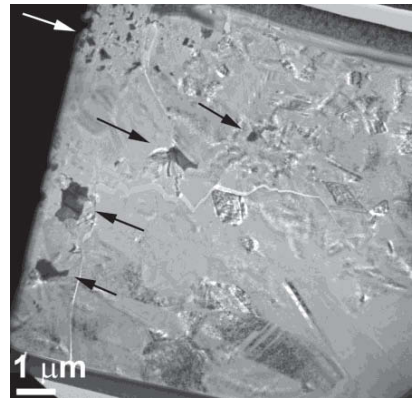


Figure 8: CP34 TEM Position 2a, showing most of the TEM sample. Dark areas indicated by arrows are precipitates.

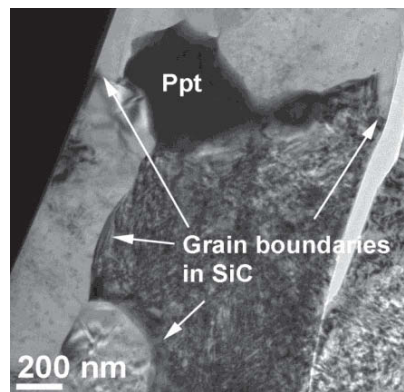


Figure 9: A higher-magnification image of the precipitate at the lower left of Figure 8, emphasizing that it is located at grain boundaries in the adjacent SiC.

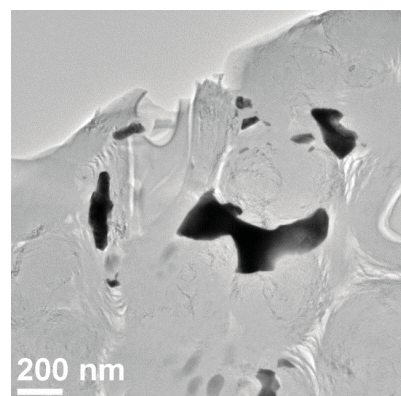


Figure 10: Dark-contrast precipitates at boundaries between spherical features in light-contrast IPyC matrix, CP34 TEM Position 1a.

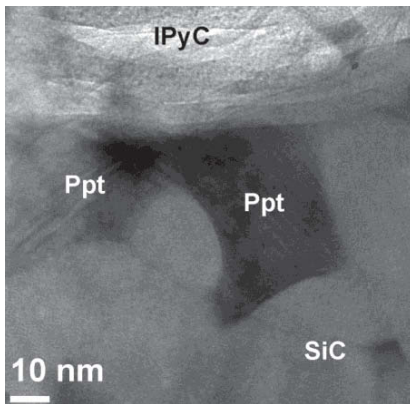


Figure 11: A nano sized precipitate at the phase boundary between IPyC and SiC, CP30 TEM Position 1a.

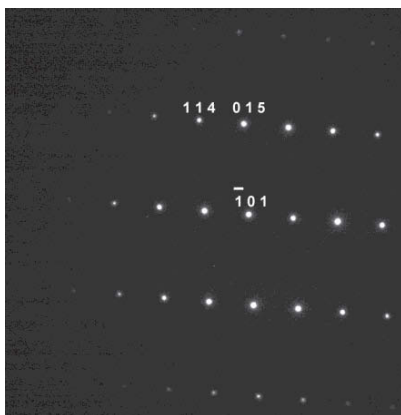


Figure 12: Selected-area diffraction pattern from precipitate shown in Figure 9, indexed as  $UPd_2Si_2$  zone axis

Specimens at Positions 1a, 1b and 2a were oriented tangent to the SiC-IPyC interface whereas TEM specimens at Positions 2b, 2c and 3 were taken perpendicular to the SiC-IPyC interface in a region where significant Pd-rich precipitates were found with SEM/EDX analysis. The rationale for specimens at Positions 2a, 2b, and 2c was to enable a TEM analysis of the precipitates through the full thickness of the SiC layer to provide information at a higher resolution than what is available with the SEM precipitation map. Although it was discovered based on the SEM evaluation that the precipitates are present in the SiC layer up to a maximum depth of 15.3  $\mu m$ , it is important to evaluate this finding at the higher magnification that the TEM analysis can provide.

The TEM micrographs in Figure 13 show that precipitates are visible in Positions 2a and 2b, but no precipitates were observed at position 2c. Position

2c is on the outer edge of the SiC layer, including roughly the outer half of the SiC layer from the midpoint,  $\sim 17 \mu m$  from the IPyC-SiC interface to the SiC-OPyC interface. This finding is in agreement with the SEM analysis discussed in section III.A., which indicates a maximum penetration of precipitates into the SiC layer of about 15  $\mu m$ .

The specimen from TEM position 2b was removed from the SiC layer immediately adjacent to and perpendicular to the IPyC-SiC interface. The precipitates found in the SiC layer at this location were identified as containing Pd and U using TEM-EDX analysis. EDX spectra also showed Si and C, however, it was not possible to determine whether these elements were from the precipitates or the matrix.

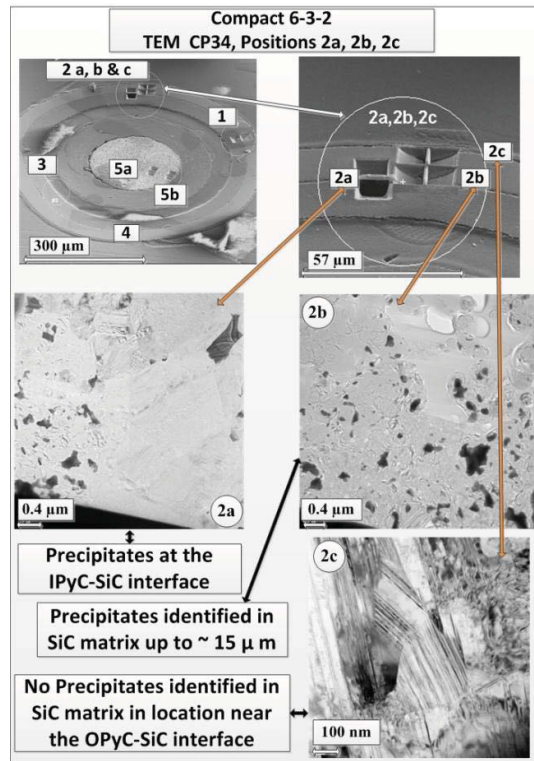


Figure 13: TEM micrographs in Positions 2a, 2b, and 2c showing that precipitates are visible in Positions 2a and 2b, but no precipitates were observed at Position 2c (dark areas in Positions 2a and 2b are precipitates).

### III.C. Pu Identification in Pd-rich Precipitates

Figure 14 shows TEM micrographs of precipitates in the IPyC layer of CP34 from Compact 6-3-2,

TEM Position 1a. Pd, U and Si were identified in spectra from these precipitates using TEM-EDX. Small peaks from Pu were qualitatively visible in almost all EDX spectra from Pd-rich precipitates from CP34 and CP35. Detection of Pu was complicated by a peak overlap between the Pu  $L\alpha$  and Sr  $K\alpha$  peaks, which was resolved by identification of the Pu  $L\beta$  peak. Detection of Pu was also complicated by the small sizes of all of the Pu peaks, and by the low numbers of counts in many of the spectra. The EDX spectra from most CP30 precipitates did not show these peaks.

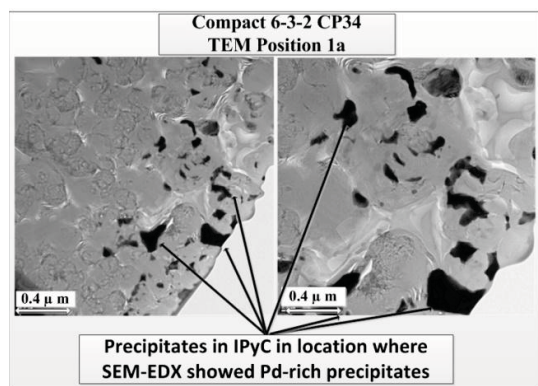


Figure 14: TEM micrograph showing representative images of precipitates in the IPyC layer of CP34 from Compact 6-3-2, TEM Position 1a.

### III.D. Ag Identification in Pd-rich Precipitates

Because of the relatively high release of silver from some of the AGR-1 fuel compacts and particles [2] and a need to better understand silver transport in the TRISO coating layers, this analysis attempted to determine whether silver was present in any of the precipitates. Detection of low concentrations of Ag in the presence of U and Pd is particularly challenging because all of the major Ag X-ray peaks with energies below  $\sim 20$  keV have energies that are similar to those from high-relative-intensity peaks from U or Pd, making it impossible to qualitatively detect Ag using EDX. Figure 15 is an expanded section of the EDX spectrum of a precipitate in the SiC layer of an irradiated AGR-1 coated particle (CP30) from Compact 6-3-2, showing the details of overlaps between Ag, Pd and U.

WDX has much higher energy resolution than EDX, and therefore could be used to distinguish between Pd and Ag. The Ag  $L\beta$  X-ray is the best

choice for WDX maps because it is separated by 78 eV from the closest Pd X-ray (Pd  $L\beta_3$ , at 3.072 keV). However, it is only 9.6 eV from the closest U X-ray (U  $Ma_2$ , at 3.1596 keV). WDX detectors can distinguish between peaks that are  $\sim 5$ -10 eV apart, depending on the relative proportions of the elements present in the sample. However, none of the WDX analysis performed to date has definitively revealed the presence of Ag in the precipitates.

Efforts to detect Ag in the precipitates continue as part of the AGR-1 PIE. A new silicon-drift EDX detector with a normal 0-40 keV range was recently installed on the TEM. This detector can be used to look for higher-energy Ag peaks (for example, the Ag  $K\alpha_1$  peak at 22.166 keV as shown in Figure 15), avoiding problems with overlaps between U, Pd, and Ag. Additional analytical techniques like local electron atom probe (LEAP) and electron energy loss spectroscopy (EELS) will also be utilized.

Although it is not possible to determine from the EDX data obtained from 0-20kV detector whether low concentrations of Ag are present in the precipitates, the gamma counts show that Ag is present somewhere in the particles [2]. Therefore, it may be useful to speculate about whether it could be incorporated into  $UPd_2Si_2$ . A number of ternary silicides with  $ThCu_2Si_2$ -type structure (body-centered tetragonal, space group  $I4/mmm$ ) have been synthesized [7–11]. These silicides have the general formula  $RX_2Si_2$ , where R is U, Th, or Gd and X is a 4d transition metal such as Cr, Mn, Fe, Co, Ni, Cu, Ru, Rh, Pd, Ir, Pt, or Au. Specific examples include  $UPd_2Si_2$  and  $GdAg_2Si_2$ . Although we are not aware of any reported syntheses of  $UAg_2Si_2$ , it seems plausible that it would also have a  $ThCu_2Si_2$ -type structure.

Since Ag and Pd have identical atomic radii (both 0.144 nm for the pure elements [12]), it seems reasonable to speculate that any Ag atoms that might be present would substitute for Pd atoms in a  $U(Ag,Pd)_2Si_2$  solid solution rather than forming a separate phase. U and Pu often substitute for one another in metals and intermetallics, and it seems reasonable to speculate that low concentrations of Pu could substitute for U in  $UPd_2Si_2$ .

### III.E. Cs-containing Precipitates

Cs-containing precipitates were observed in a worm-like feature in the interlayer area between the IPyC and SiC in CP35 (Compact 6-3-2) as shown in Figure 16. Some other Cs-rich nano-sized precipitates were also noted during the TEM evaluations and have not yet been completely

characterized. These precipitates are present inside the SiC grains and not collected as larger precipitates at the grain boundaries. These are the only Cs-rich precipitates that were identified in the TEM samples examined.

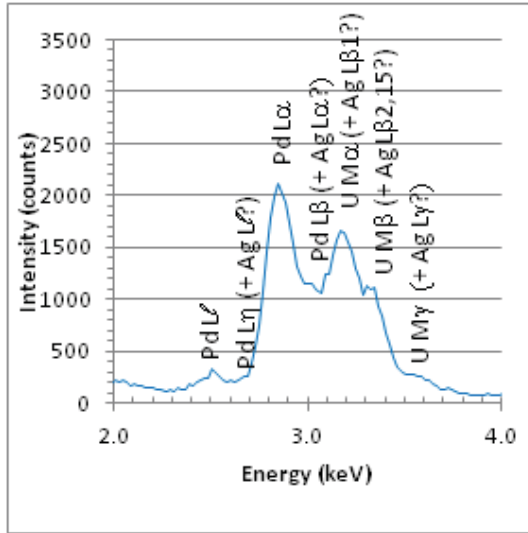


Figure 15: Expanded section of EDX spectrum showing that all Ag peaks are overlapped by those of Pd and U.

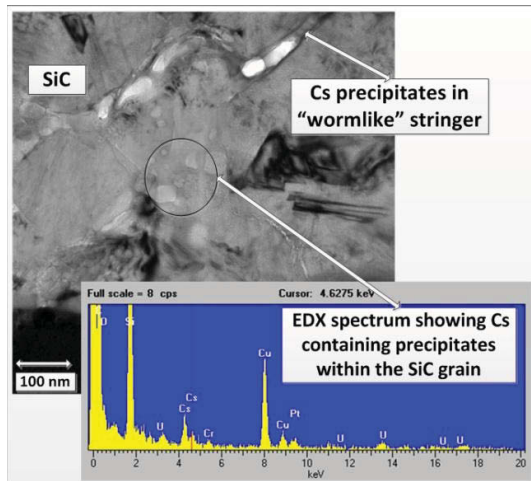


Figure 16: Bright field TEM micrograph with EDX spectra showing apparent Cs-containing precipitates in individual SiC grains and Cs-rich precipitates in the wormlike structure cross cutting various SiC grains of CP35 at Position 6 (Cu, Cr, and Pt on the EDX spectrum are artifacts).

### III.F. SiC Microstructure

Preliminary TEM analysis of the irradiated SiC showed irregular shaped crystals ranging in size from <100nm to several micrometers across. Twinning, stacking faults, and dislocations are common in SiC. It is not possible to determine from the present data whether the SiC has a preferred orientation. As expected, no evidence was found of any phase transformation of SiC from the cubic to the hexagonal phase because of irradiation as determined by selected area diffraction (SAD) patterns measured on the different TEM samples prepared from CP34 and CP35. It is expected that EBSD analysis of these layers will provide more statistical data on the presence of hexagonal phases that may have formed during irradiation. This analysis needs to be completed with comparative datasets from equivalent unirradiated particles. Detailed studies on the grain size distribution, orientation and microstructure comparing unirradiated with irradiated SiC layers of these coated particles will be discussed in a separate publication at a later stage.

Although a full investigation was not completed on loop and dislocation densities of this material, no significant difference through the thickness of the SiC layer for CP34 was observed at one specific position. However, differences were observed at different locations on the circumference of the SiC layer. No denuded zone for dislocation loops along grain boundaries were observed during this study, but previous studies have typically reported denuded zones at grain boundaries in some areas for irradiated SiC at 1130°C [13]. This distribution of dislocation loops may be important to understand the fission product transport mechanisms and therefore will be investigated specifically in the areas where fission product precipitates were found. At this point no conclusion has been reached from this observation and additional analysis is needed.

Cavities were predominantly found to be spherical in shape for CP34 (Figure 17) in contrast with angular shaped cavities found in CP35 (Figure 18). Further work is required to understand areas where cavities are only visible on one side of a grain boundary as shown in Figure 17. At present, information on cavity or void formation in irradiated chemical vapor deposited 3C SiC are very limited. However, these AGR-1 PIE studies will be used to further establish information on cavities in the irradiated microstructure. Kondo *et al.* [13] typically found that the shape of cavities change from spherical to faceted as a function of irradiation

temperature and the transition typically occurs at 1400°C.

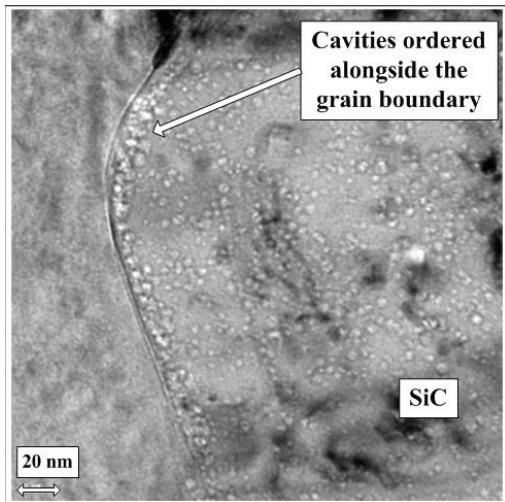


Figure 17: Spherical shaped cavities concentrated alongside grain boundaries of Compact 6-3-2 CP34 TEM sample 2a near a Pd-rich precipitate.

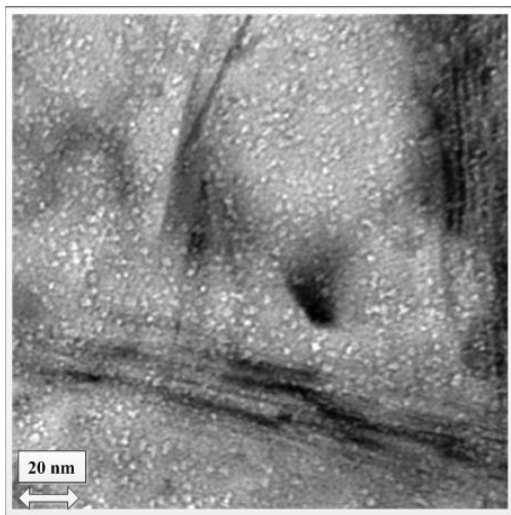


Figure 18: Bright field TEM image of the irradiated SiC microstructure of CP35 showing that the cavities are angular shaped.

### III.G. IPyC Microstructure

Very preliminary TEM observations of the IPyC layer in unirradiated coated particles showed randomly oriented crystallites 5-10 nm across (Figure 19), becoming less random near the interface with the SiC. The corresponding selected area diffraction pattern for the unirradiated fuel is shown

in Figure 19. Although more detailed work is in process to fully quantify the isotropic nature of the IPyC as a function of the four aperture diameters as proposed by Helary *et al.* [14], some preliminary observations were made. Diffraction patterns from both the unirradiated and irradiated AGR-1 Baseline IPyC showed four rings whose radii correspond to d-spacings of approximately 3.45, 2.08, 1.69, and 1.21 Å. Variations in intensity around the rings in the experimental diffraction patterns indicate preferred orientation. Diffraction patterns taken with the smallest available selected-area aperture (effective diameter ~160 nm), commonly show large variations in intensity in the smallest ring, indicating a high degree of preferred orientation. These variations become "averaged out" in diffraction patterns with the largest aperture (effective diameter ~1200 nm).

Preliminary evaluation on the irradiated IPyC shows variation in intensity going around each ring. Although intensity variations within individual rings in the IPyC diffraction patterns after irradiation are observed for CP34 and CP35 (Figures 20 (a), (b) and (c)) and are an indication that the IPyC is becoming anisotropic, no final conclusion can be made as a more detailed analysis is needed. For example, SAD patterns needs to be measured as a function of distance from the IPyC-SiC interlayer and aperture diameters. At this point, it cannot be concluded whether temperature or neutron fluence is the predominant reason for the observed changes. However, previous research by Van Rooyen *et al.* [15] implies that it may be predominantly because of the temperature effect. More information and examination are needed to determine whether these differences are significant.

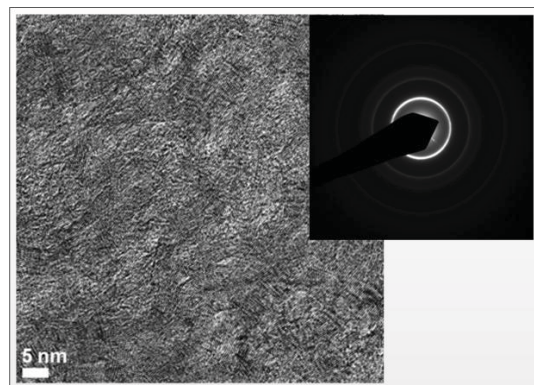


Figure 19: Image of unirradiated IPyC showing randomly oriented crystals 5-10 nm across with corresponding SAD pattern.

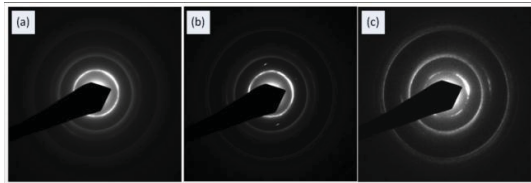


Figure 20. Selected area diffraction patterns as examples of preliminary data on IPyC structure of (a) CP34 Position 1a (b) CP34 Position 3 and (c) CP35 Position 6 (Aperture sizes were not recorded during time of analysis and may not be the same for all the diffraction patterns).

### III.E. IPyC–SiC Interlayer Microstructure

No evidence was observed of IPyC-SiC interface debonding in either the Compact 6-3-2 samples due to irradiation. As an example the IPyC-SiC interface in the CP35 TEM sample (Position 6) is shown in Figure 21.

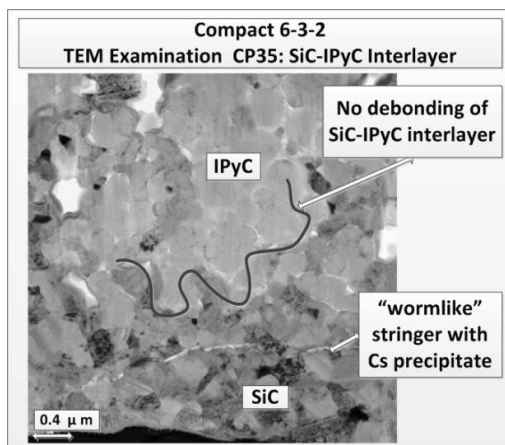


Figure 21. Bright field TEM image of the SiC-IPyC of CP35 shows no evidence of debonding.

### VI. FUTURE WORK PLANNED

The detailed analysis of the unirradiated fuel variants is in progress and will be compared with results from irradiated fuel. Specifically the IPyC-SiC interlayer properties and the IPyC characteristics will be determined and compared. In addition the electron microscopic examination of the fuel kernels will be completed and reported.

The TEM examination did not include full irradiation effects quantification and it is therefore recommended that a comparison of CP34 with CP35 be done as a follow-up study. It should be

accentuated, however, that this work needs to be approached with a more detailed focus and specific objectives, which were not included in this preliminary study.

EPMA is a recommended WDX technique for determining both qualitative and quantitative concentrations of Ag. This technique will be used for analysis of irradiated particles from other compacts.

Recommendations include the verification of precipitate composition using TEM EDX with X-ray energies of 0-40 keV to differentiate between Ag, Pd, and U. It is also recommended that a detailed precipitate analysis be done using EPMA and LEAP techniques, in conjunction with more in-depth investigation on the presence of fission products in intergranular and transgranular locations in the SiC.

Future work includes also a more detailed and quantitative study on cavities and dislocation loops. This may provide information on the relationship between cavity formation and grain orientation and if a possible link exists between these characteristics and precipitate locations.

Quantifying the PyC anisotropy on irradiated material is recommended because it may be significant to be able to use apparent anisotropy as an indicator of relative temperature. However the challenge remains to overcome the variability of the unirradiated particles due to the inherent manufacturing properties and then to quantify the anisotropy in a specific particle after irradiation. The role of neutron irradiation on the anisotropy of PyC also needs to be confirmed.

### IV. CONCLUSIONS

TEM analyses showed two kinds of precipitates: one with Cs, and one with U, Pd, and Si. The Cs precipitates were observed in a worm-like structure at the IPyC-SiC interface in CP35 (Compact 6-3-2) only. The Pd-rich precipitates are randomly distributed around the circumference of the particle cross section in the SiC-IPyC interlayer and are present in both the SiC and IPyC layers. The precipitates in the SiC extended a distance of ~15.3 μm and 17.5 μm from the IPyC-SiC interlayer, respectively, for Compact 6-3-2 CP34 (11.3% FIMA) and Compact 4-1-1 CP21 (19.3% FIMA). No significant Pd corrosion of the SiC layer was observed. The following preliminary conclusions can be reached from the Pd-rich precipitates:

- Pd-rich precipitates were found at grain boundaries.

- TEM/EDX spectra from Pd-rich precipitates show U, Pd, and Si. Some of the Si may be from the SiC for precipitates in the interlayer and SiC layers. Many precipitates (particularly in CP34 and CP35) show Pu and a few show Zr.
- While no evidence of Ag was found in the precipitates, it is not possible at this time to definitively conclude that it is not present because of overlaps between Ag x-ray peaks and those of Pd and U.
- Preliminary TEM (EDX+SAD) phase identification suggests that the precipitates have a structure similar to that of UPd<sub>2</sub>Si<sub>2</sub>. However the proportions of U and Pd do not match this stoichiometric composition.
- No significant differences are observed between the Pd-rich precipitate location and distribution of coated particles from Compact 6-3-2 and Compact 4-1-1. Nano-sized precipitates are observed in the SiC layer up to a depth of 15.3 and 17.5 μm for those two compacts respectively

As expected, no SiC phase transformation due to irradiation is observed in any of the Compact 6-3-2 coated particles examined.

#### ACKNOWLEDGMENTS

This work was supported by the U.S. Department of Energy, Office of Nuclear Energy, under DOE Idaho Operations Office Contract DE-AC07-05ID14517. Jim Madden, Scott Ploger and Jason Harp are acknowledged for their contributions towards the SEM/TEM sample preparation.

#### REFERENCES

- [1] J. Simonds, “Technical Program Plan for the Next Generation Nuclear Plan/Advanced Gas Reactor Fuels Development and Qualification Program, PLN-3636, Rev. 0, September 2010.
- [2] P.A. Demkowicz, J.D. Hunn, R.N. Morris, J.M. Harp, P.L. Winston, C.A. Baldwin, F.C. Montgomery, Preliminary Results of Post-Irradiation Examination of the AGR-1 TRISO Fuel Compacts, HTR2012-3-021
- [3] J.T. Maki, AGR-1 Irradiation Experiment Test Plan, INL/EXT-05-00593 Rev. 3, Idaho National Laboratory (INL), 2009.
- [4] M. Barrachin, R. Dubourg, S. de Groot, , M.P. Kissane, , K. Bakker, “Fission-product behavior in irradiated TRISO-coated particles: Results of the HFR-EU1bis experiment and their interpretation,” *Journal of Nuclear Materials*, Vol. 415, 2011, pp. 104–116
- [5] J.B. Kortright, and A.C. Thompson, “X-Ray Emission Energies,” X-Ray Data Booklet 2009 [cited 2011 December 5, 2011]; Available from: [http://xdb.lbl.gov/Section1/Sec\\_1-2.html](http://xdb.lbl.gov/Section1/Sec_1-2.html).
- [6] J. Goldstein, et al., *Scanning Electron Microscopy and X-Ray Microanalysis*, Third Edition ed. 2003, New York, NY: Springer.
- [7] B. Shemirani, et al., “Magnetic structure of UPd<sub>2</sub>Si<sub>2</sub>,” *Physical Review B*, 1993, Vol. 47, Issue 13.
- [8] J. Leciejewicz, H. Ptasiwicz-Bak, and A. Zygmunt, “Magnetic phase transitions in UPd<sub>2</sub>Si<sub>2</sub>,” *J. Phys. Stat. Sol. (a)*, Vol. 51, 1979, pp. K71–K73.
- [9] H. Ptasiwicz-Bak, J. Leciejewicz, and A. Zygmunt, “Neutron diffraction study of magnetic ordering in UPd<sub>2</sub>Si<sub>2</sub>, UPd<sub>2</sub>Ge<sub>2</sub>, URh<sub>2</sub>Si<sub>2</sub>, and URh<sub>2</sub>Ge<sub>2</sub>,” *J. Phys. F: Metal Phys.*, Vol. 11, 1981, pp. 1225-12
- [10] R. Marazza, et al., “Some phases in ternary alloys of thorium and uranium with the Al<sub>4</sub>BaThCu<sub>2</sub>Si<sub>2</sub>-type structure,” *Journal of the Less-Common Metals*, Vol. 53, 1977, pp. 193–197.
- [11] K.H. JBuschow and D.B. De Mooij, “Structural and magnetic characteristics of several ternary compounds of the type GdX<sub>2</sub>Si<sub>2</sub> and UX<sub>2</sub>Si<sub>2</sub> (X=3d, 4d, or 5d metal),” *Philips Journal of Research*, Vol. 41, 1986 pp. 55–76.
- [12] E.A. Brandes and G.B. Brook, eds., *Smithells Metals Reference Book*, Seventh Edition, 1992, Butterworth-Heinemann, Ltd.: Oxford.
- [13] S. Kondo, Y. Katoh, L. L. Snead, “Microstructural defects in SiC neutron irradiated at very high temperatures,” *Journal of Nuclear Materials*, Vol. 382, 2008, pp. 160–169.
- [14] D. Helary, O. Dugne, X. Bourrat, Advanced characterization techniques for SiC and PyC coatings on high-temperature reactor fuel particles. *Journal of Nuclear materials*, 337 (2008) 150-156
- [15] I.J. van Rooyen, J. Neethling, and J. Mahlanghu, “Influence of temperature on the micro- and nanostructures of experimental PBMR TRISO coated particles: A comparative study,” HTR2008-58189, Proceedings of the 4th International Topical meeting on High Temperature Reactor Technology, HTR2008, September 28- October 1, 2008, Washington, DC USA.